View Article Online
View Journal

Journal of Materials Chemistry A

Accepted Manuscript

This article can be cited before page numbers have been issued, to do this please use: M. Bagherzadeh, R. Kaveh and H. Mahmoudi, *J. Mater. Chem. A*, 2019, DOI: 10.1039/C9TA02882J.

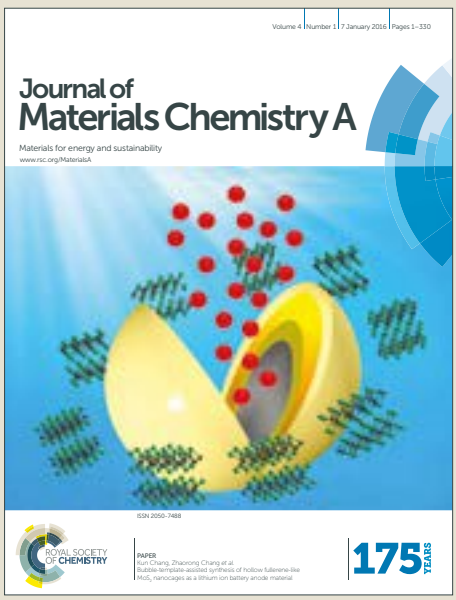

ROYAL SOCIETY OF CHEMISTRY

rsc.li/materials-a

Journal of Materials Chemistry A
View Article Online
DOI: 10.1039/C9TA02882J

Facile synthesis of recyclable Pd-rGO/CNT/$CaFe_2O_4$ nanocomposite with high multifunctional photocatalytic activities under visible light irradiation

Mojtaba Bagherzadeh,*[a] Reyhaneh Kaveh [a] and Hamed Mahmoudi [a]

[a] *Chemistry Department, Sharif University of Technology, Tehran, P.O. Box 11155-3615, Iran;* bagherzadeh@sharif.edu

Abstract:

We report a facile method to synthesize a magnetically separable Pd-rGO/CNT/$CaFe_2O_4$ photocatalyst. The incorporation of CNTs into rGO can be performed with a conductive network structure to bridge between the gaps of rGO sheets. This conductive network can prevent the restacking of GO nanosheets during the reduction process. Also, for photocatalysis, the aforementioned conjugated network can provide rapid electronic conducting channels. It was found that the Pd-rGO/CNT/$CaFe_2O_4$ nanocomposite is an efficient photocatalyst for Heck-Mizoroki coupling reaction under irradiation of visible light. Interestingly, the electrons which exited by the photon can be transferred to the palladium nanoparticles causes an increase in the electron density of Pd in consequence increases the catalytic activity of these nanoparticles in Heck-Mizoroki coupling reactions under visible light. In this regard, we tested the catalytic activity of these nanocomposites in Heck-Mizoroki coupling reaction under visible light to obtain the product in good to excellent yields. As compared to pure $CaFe_2O_4$, rGO/$CaFe_2O_4$, and rGO/CNT/$CaFe_2O_4$ nanocomposites, the prepared Pd-rGO/CNT/$CaFe_2O_4$ photocatalyst exhibits remarkably increased photocatalytic degradation of methylene blue (MB). The presence of Pd nanoparticles can act as a co-catalyst and delay the recombination of photoinduced electron-hole pairs of $CaFe_2O_4$.
Keywords: *Photocatalyst, rGO, CNT, Pd, $CaFe_2O_4$, photocatalytic Heck-Mizoroki coupling, MB degradation*

1. Introduction

Solar energy as a renewable source of energy plays an important role in acquiring higher activity without high energy consumption. In other words, coupling solar energy with active catalysts enhances the overall performance of the catalysts and environmental protection.[1] The field of heterogeneous photocatalysis has been studied for nearly four decades due to their interesting advantages in the sustainable transformation of organic molecules.[2] Recently, the interest in photocatalysis has concentrated on the use of semiconductor materials. Most of the organic reactions are performed exposure heating condition, which is energy intensive.[3] One of the twelve principles of green chemistry is to minimize the energy requirements of chemical processes so it would be an outstanding breakthrough if the catalytic reaction can be performed at room temperature under visible light irradiation.[4] Considering the explosive growth of green and environmentally benign synthetic process, light-catalyzed chemical reactions have attracted a lot of attention as zero valent metal nanoparticles, especially Pd nanoparticles can be used as a catalytically active species for a great number of main chemical reactions.[5]

The palladium-catalyzed Heck-Mizoroki coupling reaction is one of the most important carbon-carbon coupling reactions with a considerably wide scope in organic synthesis. Also, this coupling reaction has been extensively used for the synthesis of pharmaceuticals, polymers and natural products.[6] Conventional Pd catalysts for Heck-Mizoroki coupling reaction which has been widely investigated are mostly inhomogeneous with different additives or ligands.[3b, 3d-h] Most of the time, these reactions require difficult conditions, such as high temperature and long reaction

View Article Online
DOI: 10.1039/C9TA02882J

time.[7] Difficult separations and the poor thermal stability of these Pd catalysts significantly hinder their applications in the chemical industry. Although heterogeneous catalysts can overcome those challenges, they are generally less efficient than their homogeneous counterparts. In addition, a great number of heterogeneous catalysts have difficulties in their separation from the mixture of reaction by centrifugation and filtration.[3a, 8] These problems would be removed by preparation of magnetic catalysts that can be easily separated by an external magnet from the mixture of reaction.

Many works are available on the Heck-Mizoroki coupling reaction in which palladium was supported on different silica, zeolite, metal oxides and carbon-based materials.[9] Carbon-based materials such as graphene oxide and carbon nanotubes can be good choice as support for palladium nanoparticles due to their unique properties including the high surface area, morphology, good chemical stability, and good electrical conductivity.[10] According to the previous studies, nanosheets of graphene and its derivatives show superior mechanical and chemical properties also, extraordinary interaction with the loaded nanoparticles and good conductivity for electron capture and transport make them effective in catalysis, pollutant degradation, etc.[11] However, graphene-based materials are very easily aggregated due to the π-π stacking interaction between the sheets. Consequently, the further modification should be carried out to remove this problem. In fact, the rGO/CNT network as a catalyst supporting material has been used for preparing of this nanocomposite. Introduction of CNT between sheets of graphene via van der Waals forces, hydrogen bonding, and π-π stacking can bridge the adjacent sheets of graphene, avoiding graphene sheets aggregation and increase the conductivity and specific surface area.[12] Supporting Pd nanoparticles on rGO/CNT composite not only provide a large surface area but also increase thermally stable system.[13]

The interest in photocatalysis has concentrated on the use of semiconductor materials recently. In fact, a great number of semiconductor materials have been used as photocatalysts for environmental protection.[14] The large band gap semiconductors, such as titanium oxide (TiO_2),[15] zinc oxide (ZnO),[16] strontium titanate ($SrTiO_3$),[17] and Zinc sulfide (ZnS),[18] are capable of utilizing only a small portion of sunlight (UV light), while spinel ferrites (MFe_2O_4) can effectively utilize visible light due to their narrow band gaps.[19] In addition, recovery and reusability of the photocatalysts are very important.[20] The magnetic property of the spinel ferrites is another reason for making them useful in preparing of the photocatalysts.[21] Therefore, MFe_2O_4 as magnetic materials with thermally and chemically stabilities and narrow band gaps have been used for preparing of effective photocatalysts.[22] The nontoxic and inexpensive $CaFe_2O_4$, as a member of the spinel ferrites, has paid lots of attention because of the interesting catalytic and magnetic properties. This narrow band-gap semiconductor is found to be a perfect photocatalyst under visible-light irradiation.[23]

However, spinel ferrites cannot exhibit satisfied photocatalytic performance alone. This issue is related to the high recombination rate of photoinduced electron-hole pairs. One of the best ways to solve this problem is to combine spinel ferrites with carbon-based materials such as porous carbon,[24] carbon nanotubes (CNTs)[13a, 13b], and graphene.[13c-f] Unique physicochemical properties

View Article Online
DOI: 10.1039/C9TA02882J

of carbon materials make them perfect supporting materials for various nanoparticles loading, such as spinel ferrites, to improve their photocatalytic performance. Among different carbon-based materials, carbon nanotubes and graphene sheets show a promising performance due to their high specific area, corrosion resistance, and intrinsic excellent conductivity.[25]

In this report, we successfully synthesized quadruple Pd-rGO/CNT/$CaFe_2O_4$ nanocomposite as an effectiveness photocatalyst for Heck-Mizoroki coupling reaction at room temperatures under irradiation of visible light. Also, the prepared photocatalyst can be easily separated from the system of reaction via an external magnetic. We also demonstrate that Pd-rGO/CNT/$CaFe_2O_4$ nanocomposite photocatalyst exhibits remarkably increased photocatalytic methylene blue (MB) degradation as compared to pure $CaFe_2O_4$, rGO/$CaFe_2O_4$, and rGO/CNT/$CaFe_2O_4$ nanocomposites. MB is one of the most dangerous pigments which are important pollutants in the wastewater of a great number of industries like textiles and chemicals.[14]

Experimental

2.1. Preparing of rGO/CNT nanocomposite

1 g of the purchased MWCNTs were suspended in 200 mL of a mixture of concentrated H_2SO_4 (98 wt%) and HNO_3 (65 wt%) with a volume ratio of 3:1 and then was sonicated for 3 h. The obtained solid was collected by centrifugation, washing repeatedly with distilled water until the pH of 7 and drying at 80 °C for 5 h under vacuum. The purpose of CNTs treatment is removing the impurity and functionalize the surface of CNTs. Also, Graphene oxide (GO) synthesized from purified graphite powder by using the Hummers method.[26] Then 120 mg of acid-treated CNTs were added into the 60 mL of homogeneous GO aqueous dispersion (2 mg/mL). In order to develop an interconnected structure between GO and acid-treated CNTs, they mixed together with a mass ratio of 1:1. After being sonicated for 30 min, the mixture was transferred into a 100 mL sealed Teflon-lined autoclave for 12 h at 180 °C. Finally, the obtained mixture was cooled in room temperature and the black-colored rGO/CNT nanocomposite was collected.

2.2. Preparing of Pd-rGO/CNT nanocomposite

A 50 mL round-bottom flask equipped with a magnetic stirrer was charged with $PdCl_2$ (72 mg, 0.4 mmol) and KCl (668 mg, 9 mmol), in 15 mL water. The flask was heated at 80 °C until $PdCl_2$ was dissolved. This solution was cooled at room temperature and added dropwise to a suspension of rGO/CNT (400 mg) in 15 mL water. The suspension was stirred at room temperature for 2 h, then filtered under reduced pressure, washed with water and methanol and dried in air. The product Pd-rGO/CNT was obtained as a black solid.

2.3. Preparing of Pd-rGO/CNT/$CaFe_2O_4$ nanocomposite

To synthesize the $CaFe_2O_4$ nanoparticles, calcium nitrate $Ca(NO_3)_2.6H_2O$ and ferric nitrate $Fe(NO_3)_3.9H_2O$ with a molar ratio of (1:2) were dissolved in 60 mL ethylene glycol (EG) and the mixture was sonicated for 10 min. An appropriate KOH solution was used to adjust the

View Article Online
DOI: 10.1039/C9TA02882J

pH of the solution to 10. Then the resulting mixture was sealed in a 100 mL Teflon-lined autoclave and maintained at 125 °C for 24 h. After collection and being washed with ethanol, the product was dried and the brown-colored $CaFe_2O_4$ nanoparticles were obtained. The Pd-rGO/CNT/$CaFe_2O_4$ nanocomposite with various loadings of $CaFe_2O_4$ was prepared using the following procedure. 0.5 g of Pd-rGO/CNT and various weight percents of $CaFe_2O_4$ (30%, 40%, and 50%) were dispersed in 60 mL of ethanol by sonication for 2 h. In order to get a homogeneous suspension, the resulting mixture kept under continuous stirring for 12 h. Then the suspension was transferred into a 100 mL Teflon lined autoclave. The autoclave was sealed and maintained at 120 °C for 6 h. The final product was centrifuged and dried at 70 °C in an oven. The loading of Pd was determined to be 1.72% w/w Pd by ICP-OES analysis. For comparison, rGO/$CaFe_2O_4$ and rGO/CNT/$CaFe_2O_4$ were synthesized using the same preparation method of Pd-rGO/CNT/$CaFe_2O_4$ without the addition of Pd in both composites (rGO/$CaFe_2O_4$ and rGO/CNT/$CaFe_2O_4$) and acid treated MWCNT in first composite (rGO/$CaFe_2O_4$). The synthesis process for the Pd-rGO/CNT/$CaFe_2O_4$ nanocomposite is depicted in scheme 1.

2.4. Photocatalytic Heck-Mizoroki Reaction

In a 25 mL round bottom flask equipped with a magnetic stirrer, aryl iodide (1 mmol), alkene (1.2 mmol), TEA (1.5 mmol), catalyst (0.1 mol%, 6.2 mg) and dimethylacetamide (DMA, 1 M, 1 mL) were consecutively added and the resulting mixture was left under visible light illumination (a 250-W mercury lamp with the UV cut-off filter). The distance between the aforementioned flask and the light source were 50 cm and the reaction temperature was maintained at (25 °C ± 2 °C) by using a water bath circulator system. The reaction monitored by gas chromatography system. A Parallel reaction was performed as a dark control under the same condition in a dark environment to check the ability of photocatalyst in the transformation of organic materials in Heck–Mizoroki coupling reaction.

2.5. Thermocatalytic Heck-Mizoroki Reaction

In a 5 mL round bottom flask equipped with a magnetic stirrer and condenser, aryl iodide (1 mmol), alkene (1.2 mmol), TEA (1.5 mmol), catalyst (0.1 mol%, 6.2 mg) and dimethylacetamide (DMA, 1 M, 1 mL) were consecutively added and the resulting mixture was left under stirring at 130 °C and the reaction monitored by gas chromatography system.

2.6 General procedure for extraction work-up of catalytic product in Photocatalytic and Thermocatalytic Heck-Mizoroki Reaction

After 5h, the catalyst was separated by using an external magnetic field, and 2 mL of Ethyl acetate was added to the remain solution. The liquid extraction was performed by adding water (3×2 mL) to extracting dimethylacetamide. Finally, the product was obtained by distillation of Ethyl acetate. Final purification of the catalytic product was performed by using flash chromatography.

2. Results and discussion

3.1. Characterizations

View Article Online
DOI: 10.1039/C9TA02882J

The prepared materials were characterized by using several techniques such as FT-IR, PXRD, Raman, Magnetometer, electrochemical impedance spectroscopy, and Photoluminescence. Full characterization details are available in supporting information.

To investigate the morphologies of the synthesized F-MWCNT, rGO/CNT, Pd-rGO/CNT/$CaFe_2O_4$ nanocomposites, the FESEM images of these samples are presented in Fig. 1. As observed in Fig. 1a, due to the presence of functional groups after acid treatment, the bundle-liked MWCNTs appeared dispersed. Also, white impurities were observed on the surface. In addition, the smooth wall of the MWCNTs became less smooth and a little bent because of the side attachment of the -COOH groups during acid treatment. Fig. 1b shows that F-MWCNTs were significantly distributed on the surface of GO sheets, also F-MWCNTs inserted into the GO sheets. The F-MWCNTs nanotubes can act as bridges to prevent GO sheets from restacking and increase the spaces between sheets. The presence of interaction between the synthesized nanoparticles (Pd, $CaFe_2O_4$) with the rGO/CNT nanocomposite can be vividly seen in Fig. 1-c.

The EDX spectrum of Pd-rGO/CNT/$CaFe_2O_4$ nanocomposite indicate that the elements C, O, Fe, Ca, and Pd present in this nanocomposite. The EDX-mapping (Fig. 1d-h) that is related to the FESEM image in Fig. 1c shows that the Ca, Fe and Pd Elements have a uniform dispersity in the rGO/CNT nanocomposite.

In order to investigate the optical absorption performance of the prepared samples, UV-Vis diffuse reflectance spectra (DRS) of neat $CaFe_2O_4$, rGO/CNT/$CaFe_2O_4$ and Pd-rGO/CNT/$CaFe_2O_4$ nanocomposite in Fig. 2. As can be seen in Fig. 2a, the $CaFe_2O_4$ has significant absorption in the visible region due to its narrow bandgap but after the formation of Pd-rGO/CNT/$CaFe_2O_4$, the nanocomposite exhibits increased absorption in the visible region, indicating that the Pd-rGO/CNT/$CaFe_2O_4$ nanocomposite possess better visible-light photocatalytic activity (Fig. 2c). This phenomenon not only can be related to the electronic transition between rGO/CNT and $CaFe_2O_4$ but also can be attributed to the inherent absorption of rGO/CNT nanocomposite. On the other hand, the presence of rGO/CNT nanocomposite can lead to a bridge between the $CaFe_2O_4$ and light. The DRS test for rGO/CNT/$CaFe_2O_4$ also showed that the presence of Pd nanoparticles in Pd-rGO/CNT/$CaFe_2O_4$ nanocomposite does not significantly change the optical properties of rGO/CNT/$CaFe_2O_4$ nanocomposite (Fig 2b).

3.2. Catalytic activity in Heck-Mizoroki coupling reactions

Since Pd is widely known to be a catalytically active species for a large number of organic reactions under thermal conditions, for finding the ability of the catalytic system in the cross-coupling reactions, we tested the catalytic system in the Mizoroki-Heck coupling reaction. For this reason, iodobenzene and methyl acrylate were chosen as model substrates and triethylamine as a base. Interestingly, with only 0.1 mol% Pd content the reaction was completed in 5h. This result showed that this catalyst is perfect under this condition for the Heck-Mizoroki coupling reaction.

In the next step, we start to change the source of energy to the visible light and we perform one reaction under visible light, in parallel, a dark control reaction was performed with the same condition under dark environment. Surprisingly, the photocatalytic reaction showed perfect

View Article Online
DOI: 10.1039/C9TA02882J

conversion in comparison with dark control reaction. A summary of this study has been gathered in Table 1.

To verify the efficiency of the catalytic system, we investigated the Heck–Mirozoki coupling reaction using a series of aryl iodides and alkyl acrylates or styrenes (Table 2) Using both thermal and photocatalytic reaction and obtaining after 5 h with good to excellent yields of isolated products. This study Emphasis that the thermal condition slightly better than photocatalytic reaction, but photocatalytic reaction also showed very promising results and given the importance of using light rather than heat in such reactions, this catalyst can be a good alternative to the traditional thermal methods of cross-coupling reactions. The products ^{1}H NMR spectra are depicted in Fig. S17-S32 respectively (the supplementary materials).

To verify the efficiency of these well-defined materials in photocatalytic Heck-Mizoroki coupling reaction, authors made a comparison between the catalytic system introduced in this work and some other previously published photocatalytic systems. Suresh B. Waghmode et al. prepared $PdCl_2/TiO_2$ catalyst, and they showed that the catalytic activity of this heterogeneous system in Heck-Mizoroki coupling is perfect under UV-Vis light and 45°C.[27] Saurabh S. Soni et al. synthesized the Pd(0)-doped mesoporous TiO_2 nanoparticles (Pd/TiO_2) and showed that the catalytic activity of Pd/TiO_2 nanoparticles is remarkably increased under solar light irradiation for the Heck reaction.[8a] X. Wei Guo et al. showed that Pd nanoparticles, supported on carbon nanocoils (Pd/CNCs), has unexpected high photocatalytic activity for Heck coupling reaction at 40°C.[28] H. Shin et al. showed that the incorporation of MoS_2 nanosheets with Pd nanodots can be a good strategy for promoting the visible-light-induced Suzuki–Miyaura C–C coupling reaction.[1b] The results of this comparison are summarized in Table 3. These comparisons clearly show the efficiency of the present catalytic system considering TOF, which is very important in the point of view of the atom economy in green chemistry.

3.3. catalytic activity on Methylene Blue degradation

Fig. S11 shows the photocatalytic activities of prepared samples for the degradation of MB (12 mg L^{-1}, 50 mL, and 3 g L^{-1} catalyst) under visible light illumination. The obtained results show that the MB photolysis under visible light irradiation is not considered in the absence of photocatalyst. In a dark situation, no electron-hole pairs can be formed and since the photocatalytic performance of photocatalysts depends on formation, separation, and migration of charges, decomposition of MB is ignorable after 30 min. As observed, the Pd-rGO/CNT/$CaFe_2O_4$ (40%) nanocomposite exhibits higher photocatalytic activity than that of the other samples. The degradation of MB via Pd-rGO/CNT/$CaFe_2O_4$ (40%) is > 98% during 75 min however the photodegradation of MB by the pure $CaFe_2O_4$, rGO/$CaFe_2O_4$ (40%) and rGO/CNT/$CaFe_2O_4$ (40%) is 24%, 35% and 90% in 75 min, respectively. The synergistic effect of rGO and CNTs can be a good contribution to increase the photocatalytic activity of pure $CaFe_2O_4$. Also, the obtained result demonstrates that Pd-rGO/CNT shows low photoactivity, indicating that the increased photocatalytic activity of Pd-rGO/CNT/$CaFe_2O_4$ cannot be related to the intrinsic catalytic activity of Pd nanoparticles. So, Pd nanoparticles only can play a co-catalyst role in the photodegradation of MB. In other words, the presence of Pd nanoparticles can be effective for trapping the

View Article Online
DOI: 10.1039/C9TA02882J

photogenerated electrons and it can improve the separation efficiency of the charge carriers, so a higher photodegradation of MB was obtained.

In Fig. S12, the photocatalytic kinetics of the synthesized samples were also studied. K_{app} values for photodegradation of MB are gained by plotting the curve of ln (C_0/C_t) versus t. The obtained results displayed that the kinetic simulation curves are close to linear curves. So that all of the correlation coefficients (R^2) were higher than 0.9, the pseudo-first-order kinetics model significantly fit the experimental data.[29] Fig. S13 shows that the optimized photocatalyst (Pd-rGO/CNT/$CaFe_2O_4$ (40%)) has the highest removal efficiency of MB and the value of K_{app} for this photocatalyst is 0.0548 min^{-1}.

Also, the degradation of MB as a sample of pollutants was investigated quantitatively via COD method. The results are depicted in Fig. S14. The COD values of the treated MB solution were decreased and this issue shows that in the presence of Pd-rGO/CNT/$CaFe_2O_4$ (40%) nanocomposite acceptably degradation/ mineralization of MB was carried out.

3.6. Possible photocatalytic mechanism

One of the major factors for limiting the conversion efficiency of light energy is charge recombination for semiconductor photocatalysts. The synergistic effect of rGO and CNTs can be a good contribution to overcome this issue and improve the photocatalytic performance. In fact, the incorporation of CNTs into rGO not only can be caused a conductive network structure in order to bridge between the gaps of rGO sheets but also can prevent the restacking of GO nanosheets during the reduction. This conjugated network remarkably enhances the electrical conductivity. Also for photocatalysis, this conjugated network can provide rapid electronic conducting channels. In addition, Pd nanoparticles are an effective material for trapping the photogenerated electrons because of their electron reservoir capacity so, facilitating the photodegradation of organic pollutants such as MB and enhancing photocatalytic performance. In other words, Pd nanoparticles can play as a co-catalyst role in the photodegradation of MB and these nanoparticles can delay the recombination of photoinduced electron-hole pairs of $CaFe_2O_4$.

The photoinduced electrons react with surface adsorbed O_2 to generate $O_2^{-\bullet}$, that then react with H^+ to generate $^{\bullet}OOH$, followed by rapid decomposition to $^{\bullet}OH$. Additionally, the photoinduced holes could oxidize H_2O and OH^- to generate $^{\bullet}OH$ which is involved in the photodegradation process of organic pollutants. On the other hand, the process of generating $^{\bullet}OH$ radicals can occur by two pathways.[30] So, the reactive species involved in the photodegradation process are hydroxyl radicals ($^{\bullet}OH$), superoxide radicals ($O_2^{-\bullet}$) and photogenerated holes (h^+). In order to identify the role of these species taking part in the photodegradation process, 2 mmol KI (a hole (h^+) scavenger), 2 mmol BZQ (a superoxide radical ($O_2^{-\bullet}$) scavenger), 2 mmol t-BuOH (a hydroxyl radical ($^{\bullet}OH$) scavenger) were added into the photocatalytic system using Pd-rGO/CNT/$CaFe_2O_4$ (40%) nanocomposite. As observed in Fig. S15, the presence of KI hardly decreases the rate of degradation in the photocatalytic reaction. As a consequence, the h^+ cannot play an important role in the photodegradation of MB. The photodegradation rate of MB is significantly decreased in the presence of BZQ and especially t-BuOH. This issue indicates that the $O_2^{-\bullet}$ and especially $^{\bullet}OH$ is the main reactive species. In conclusion, first $^{\bullet}OH$ and second $O_2^{-\bullet}$

View Article Online
DOI: 10.1039/C9TA02882J

are the predominant reactive species for the photodegradation of MB over the Pd-rGO/CNT/$CaFe_2O_4$ (40%) photocatalyst under the visible light illumination.

To find the mechanism of visible-light-driven Heck-Mizozroki coupling reaction, a control test was carried out in order to investigate the role of the photoinduced e^-. The result showed that after adding 2 mmol of $K_2S_2O_8$ as e^- scavenger only 9% conversion was gained under visible light irradiation. According to the published literature,[20, 31] upon visible light illumination, electrons from VB of $CaFe_2O_4$ are excited into the CB of $CaFe_2O_4$ and then they easily transfer from the CB of $CaFe_2O_4$ to the Pd nanoparticles. These nanoparticles can trap the photoinduced electrons because of their e^- reservoir capacity. The photoinduced electrons that transferred onto the nanoparticles of Pd can increase the inherent catalytic activity of palladium nanoparticles. These electrons finally transferred to the carbon-iodine bond, which caused weakening of this bond (Fig. 3). When the bond is weakened, with an oxidative addition reaction, this bond is added to the palladium and generate the active species of Ar-Pd-I complex and start the traditional Heck-Mizozroki coupling cycle. The final products can be obtained by β-hydrogen elimination. Therefore, both the photoinduced electrons and energetic nanoparticles of palladium act as active centers to attack the C-I bond of aryl halide.

3.6. Reusability

Stability and reusability of the synthesized heterogeneous catalysts are crucial parameters for the practical application. Both the photodegradation of MB solution and Heck-Mizoroki coupling reaction are selected to investigate the reusability of Pd-rGO/CNT/$CaFe_2O_4$ (40%) nanocomposite under the optimized conditions. After each test, the catalyst was separated by an external magnetic field and washed several times with distilled water and dried at 90 °C. Based on the obtained results the Pd-rGO/CNT/$CaFe_2O_4$ (40%) photocatalyst can be reused ten runs for the MB photodegradation process with no significant loss in degradation efficiency (Fig. S16) and six consecutive reaction runs for the Heck-Mizoroki coupling reaction without a dramatic loss of catalytic activity (Fig. 4). It can be indicated that the synthesized photocatalyst is stable during the photocatalytic process.

3. Conclusions

The magnetically recyclable Pd-rGO/CNT/$CaFe_2O_4$ nanocomposite has been successfully synthesized by a facile method. This nanocomposite exhibits the effective photocatalytic Heck-Mizoroki coupling reaction under room temperature that can completely replace the thermocatalytic Heck reaction. Also, this nanocomposite shows increased photodegradation of organic pollutants such as MB. Both the increased photocatalytic activities are attributed to the effective electron spatial transfer route because of the Pd nanoparticles. These nanoparticles not only can act as the electron mediator on the rGO/CNT nanocomposite and $CaFe_2O_4$ but also can trap photogenerated electrons. In addition, the incorporation of CNTs into rGO can be caused by a conductive network structure to bridge between the gaps of rGO sheets and this can prevent the restacking of GO Nanosheets during the reduction. This conjugated network significantly increases the electrical conductivity and it can provide rapid electronic conducting channels. Further, the Pd-rGO/CNT/$CaFe_2O_4$ exhibits perfect reusability for both the photodegradation of

View Article Online
DOI: 10.1039/C9TA02882J

dye and photocatalytic chemical reaction. The prepared photocatalyst can be easily recovered by an external magnet.

Acknowledgments

M.B. acknowledges the research council of the Sharif University of Technology for the research funding of this work.

View Article Online
DOI: 10.1039/C9TA02882J

References

1. a) P. A. Owusu and S. Asumadu-Sarkodie, *Cogent Eng.*, 2016, **3**, 1167990; b) H. H. Shin, E. Kang, H. Park, T. Han, C.-H. Lee and D.-K. Lim, *J. Mater. Chem., A*, 2017, **5**, 24965-24971.
2. a) M. Kataria, M. Kumar, Z. Singh and V. Bhalla, *ACS Sustainable Chem. Eng.*, 2018, **6**, 8223-8229; b) Y. Soltanabadi, M. Jourshabani and Z. Shariatinia, *Sep. Purif. Technol.*, 2018, **202**, 227-241; c) P. Ma, W. Jiang, F. Wang, F. Li, P. Shen, M. Chen, Y. Wang, J. Liu and P. Li, *J. Alloys Compd.*, 2013, **578**, 501-506. d) D. Ma, A. Liu, S. Li, C. Lu and C. Chen, *Catal. Sci. Technol.*, 2018, **8**, 2030-2045. e) Y. Wang, A. Liu, D. Ma, S. Li, C. Lu, T. Li and C. Chen, *Catalysts*, 2018, **8**, 355. f) D. Ma, S. Zhai, Y. Wang, A. Liu and C. Chen, *Molecules*, 2019, **24**, 330.
3. a) M. Bagherzadeh, H. Mahmoudi, M. Amini, S. Gautam and K. H. Chae, *Sci. Iran*, 2018, **25**, 1335-1343; b) M. Amini, A. Bayrami, M. N. Marashi, A. Arab, A. Ellern and L. K. Woo, *Inorg. Chim. Acta*, 2016, **443**, 22-27; c) M. Bagherzadeh, R. Latifi, L. Tahsini, V. Amani, A. Ellern and L. Keith Woo, *Polyhedron*, 2009, **28**, 2517-2521; d) M. Bagherzadeh, F. Ashouri, L. Hashemi and A. Morsali, *Inorg. Chem. Commun.*, 2014, **44**, 10-14; e) M. Bagherzadeh, N.-a. Mousavi, M. Zare, S. Jamali, A. Ellern and L. K. Woo, *Inorg. Chim. Acta*, 2016, **451**, 227-232; f) M. Bagherzadeh, M. Amini, A. Ellern and L. Keith Woo, *Inorg. Chim. Acta*, 2011, DOI: 10.1016/j.ica.2011.10.040; g) P. Li, P.-P. Huang, F.-F. Wei, Y.-B. Sun, C.-Y. Cao and W.-G. Song, *J. Mater. Chem., A*, 2014, **2**, 12739-12745; h) P. Ju, S. Wu, Q. Su, X. Li, Z. Liu, G. Li and Q. Wu, *J. Mater. Chem., A*, 2019, **7**, 2660-2666.
4. P. T. Anastas and E. S. Beach, *Green Chemistry Letters and Reviews*, 2007, **1**, 9-24.
5. a) X. Lang, X. Chen and J. Zhao, *Chem. Soc. Rev.*, 2014, **43**, 473-486; b) F. Wang, C. Li, H. Chen, R. Jiang, L.-D. Sun, Q. Li, J. Wang, J. C. Yu and C.-H. Yan, *J. Am. Chem. Soc.*, 2013, **135**, 5588-5601; c) Z. Jiao, Z. Zhai, X. Guo and X.-Y. Guo, *J. Phys. Chem., C*, 2015, **119**, 3238-3243; d) A. Chakravarty and G. De, *Dalton Trans.*, 2016, **45**, 12496-12506; e) K. Biswas, S. Chattopadhyay, Y. Jing, R. Che, G. De, B. Basu and D. Zhao, *Ind. Eng. Chem. Res.*, 2019, **58**, 2159-2169.
6. a) S. Tang, K. Liu, C. Liu and A. Lei, *Chem. Soc. Rev.*, 2015, **44**, 1070-1082; b) G. Meng and M. Szostak, *Angew. Chem. Int. Ed.*, 2015, **54**, 14518-14522.
7. R. K. Sharma, M. Yadav, R. Gaur, R. Gupta, A. Adholeya and M. B. Gawande, *ChemPlusChem*, 2016, **81**, 1312-1319.
8. a) S. S. Soni and D. A. Kotadia, *Catal. Sci. Technol.*, 2014, **4**, 510-515; b) H. Firouzabadi, N. Iranpoor, M. Gholinejad, S. Akbari and N. Jeddi, *RSC Adv.*, 2014, **4**, 17060-17070; c) S. Moussa, A. R. Siamaki, B. F. Gupton and M. S. El-Shall, *ACS Catal.*, 2012, **2**, 145-154.
9. V. Polshettiwar, C. Len and A. Fihri, *Coord. Chem. Rev.*, 2009, **253**, 2599-2626.
10. A. V. Nakhate and G. D. Yadav, *ChemistrySelect*, 2016, **1**, 3954-3965.
11. a) A. Adán-Más and D. Wei, *Nanomaterials*, 2013, **3**, 325-356; b) C. Huang, C. Li and G. Shi, *Energy & Environmental Science*, 2012, **5**, 8848-8868.
12. a) M. Wang, Z. Ma, R. Li, B. Tang, X.-Q. Bao, Z. Zhang and X. Wang, *Electrochim. Acta*, 2017, **227**, 330-344; b) S. Tourani, A. Rashidi, A. Safekordi, H. Aghabozorg and F. Khorasheh, *Ind. Eng. Chem. Res.*, 2015, **54**, 7591-7603.
13. a) S. Li, Z. Zhao, Y. Huang, J. Di, Y. A. Jia and H. Zheng, *J. Mater. Chem., A*, 2015, **3**, 5467-5473; b) X. Cui, Y. Wang, G. Jiang, Z. Zhao, C. Xu, A. Duan, J. Liu, Y. Wei and W. Bai, *J. Mater. Chem., A*, 2014, **2**, 20939-20946; c) G. Lui, J.-Y. Liao, A. Duan, Z. Zhang, M. Fowler and A. Yu, *J. Mater. Chem., A*, 2013, **1**, 12255-12262; d) M. Bagherzadeh and R. Kaveh, *J. Photochem. Photobiol.*, 2018, **359**, 11-22; e) L. Chen, L. Xie, M. Wang and X. Ge, *J. Mater. Chem., A*, 2015, **3**, 2991-2998; f) M. Bagherzadeh, R. Kaveh, S. Ozkar and S. Akbayrak, *Res. Chem. Intermed.*, 2018, **44**, 5953-5979.
14. a) A. Ibhadon and P. Fitzpatrick, *Catalysts*, 2013, **3**, 189-218; b) L. Alamo-Nole, S. Bailon-Ruiz, T. Luna-Pineda, O. Perales-Perez and F. R. Roman, *J. Mater. Chem., A*, 2013, **1**, 5509-5516; c) X. Chen, S. Shen, L. Guo and S. S. Mao, *Chem. Rev.*, 2010, **110**, 6503-6570.

View Article Online
DOI: 10.1039/C9TA02882J

15. Z.-Q. Guo, J.-P. Zhou, L.-L. An, J.-X. Jiang, G.-Q. Zhu and C.-Y. Deng, *J. Mater. Chem., A*, 2014, **2**, 20358-20366.
16. F.-X. Xiao, *ACS Appl. Mater. Interfaces*, 2012, **4**, 7055-7063.
17. Y. Liu, L. Xie, Y. Li, R. Yang, J. Qu, Y. Li and X. Li, *J. Power Sources*, 2008, **183**, 701-707.
18. H. R. Rajabi, O. Khani, M. Shamsipur and V. Vatanpour, *J. Hazard. Mater.*, 2013, **250**, 370-378.
19. S. Ida, K. Yamada, T. Matsunaga, H. Hagiwara, Y. Matsumoto and T. Ishihara, *J. Am. Chem. Soc.*, 2010, **132**, 17343-17345.
20. Y. Li, Z. Zhang, L. Pei, X. Li, T. Fan, J. Ji, J. Shen and M. Ye, *Appl. Catal., B*, 2016, **190**, 1-11.
21. E. Casbeer, V. K. Sharma and X.-Z. Li, *Sep. Purif. Technol.*, 2012, **87**, 1-14.
22. a) D. Guin, B. Baruwati and S. V. Manorama, *J. Mol. Catal. A: Chem.*, 2005, **242**, 26-31; b) Z. Li, X. Lai, H. Wang, D. Mao, C. Xing and D. Wang, *J. Phys. Chem., C*, 2009, **113**, 2792-2797.
23. a) L. William IV, I. Kostedt, J. Drwiega, D. W. Mazyck, S.-W. Lee, W. Sigmund, C.-Y. Wu and P. Chadik, *Environ. Sci. Technol.*, 2005, **39**, 8052-8056; b) R. Dom, R. Subasri, K. Radha and P. H. Borse, *Solid State Commun.*, 2011, **151**, 470-473.
24. C. Zhang, M. Antonietti and T. P. Fellinger, *Adv. Funct. Mater.*, 2014, **24**, 7655-7665.
25. a) C. Zhang, L. Ren, X. Wang and T. Liu, *J. Phys. Chem., C*, 2010, **114**, 11435-11440; b) S.-S. Li, H.-P. Cong, P. Wang and S.-H. Yu, *Nanoscale*, 2014, **6**, 7534-7541; c) H. Lu, Y. Huang, J. Yan, W. Fan and T. Liu, *RSC Adv.*, 2015, **5**, 94615-94622; d) S. Chattopadhyay, S. Maiti, I. Das, S. Mahanty and G. De, *Adv. Mater. Interfaces*, 2016, **3**, 1600761; e) D. Sengupta, K. Bhowmik, G. De and B. Basu, *Beilstein J. Org. Chem.*, 2017, **13**, 1796-1806.
26. W. S. Hummers and R. E. Offeman, *J. Am. Chem. Soc.*, 1958, **80**, 1339-1339.
27. S. B. Waghmode, S. S. Arbuj and B. N. Wani, *New J. Chem.*, 2013, **37**, 2911-2916.
28. X.-W. Guo, C.-H. Hao, C.-Y. Wang, S. Sarina, X.-N. Guo and X.-Y. Guo, *Catal. Sci. Technol.*, 2016, **6**, 7738-7743.
29. Z. Xue, T. Wang, B. Chen, T. Malkoske, S. Yu and Y. Tang, *Materials (Basel, Switzerland)*, 2015, **8**, 6360-6378.
30. a) F. Wang, F.-L. Li, M.-M. Xu, H. Yu, J.-G. Zhang, H.-T. Xia and J.-P. Lang, *J. Mater. Chem., A*, 2015, **3**, 5908-5916; b) A. A. Dubale, I. N. Ahmed, X.-H. Chen, C. Ding, G.-H. Hou, R.-F. Guan, X. Meng, X.-L. Yang and M.-H. Xie, *J. Mater. Chem., A*, 2019, **7**, 6062-6079.
31. M. Koohgard and M. Hosseini-Sarvari, *Catal. Commun.*, 2018, **111**, 10-15.

View Article Online
DOI: 10.1039/C9TA02882J

Figure Captions:

Fig. 1. FESEM image of (a) F-MWCNT, (b) rGO/CNT (c) Pd-rGO/CNT/$CaFe_2O_4$ (40%) and EDX-mapping of C (d), O (e), Ca (f), Fe (g), and Pd (h) of Pd-rGO/CNT/$CaFe_2O_4$ (40%) nanocomposite in the green frame of (c).

Fig. 2. The UV–Vis DRS spectra of (a) $CaFe_2O_4$, (b) rGO/CNT/$CaFe_2O_4$ (40%) (c) Pd-rGO/CNT/$CaFe_2O_4$ (40%).

Fig. 3. The effect of visible light on the activation of C-I bond through transfer electron from CB of $CaFe_2O_4$ to Pd nanoparticles.

Fig. 4. Recycling studies of the Pd-rGO/CNT/$CaFe_2O_4$ (40%) catalyst in the Heck-Mizoroki coupling reaction.

View Article Online
DOI: 10.1039/C9TA02882J

Table Captions:

Table. 1. Checking the capability of Pd-rGO/CNT/$CaFe_2O_4$ as a catalyst of Heck-Mizoroki coupling in different conditions

Table. 2. Heck-Mizoroki coupling of aryl iodide with different olefins in the presence of Pd-rGO/CNT/$CaFe_2O_4$ catalyst under thermocatalytic VS photocatalytic conditions

Table. 3. A comparative study of Pd-rGO/CNT/$CaFe_2O_4$ with the previously reported catalysts in Heck-Mizoroki coupling reactions.

View Article Online
DOI: 10.1039/C9TA02882J

List of Figures:

Fig. 1.

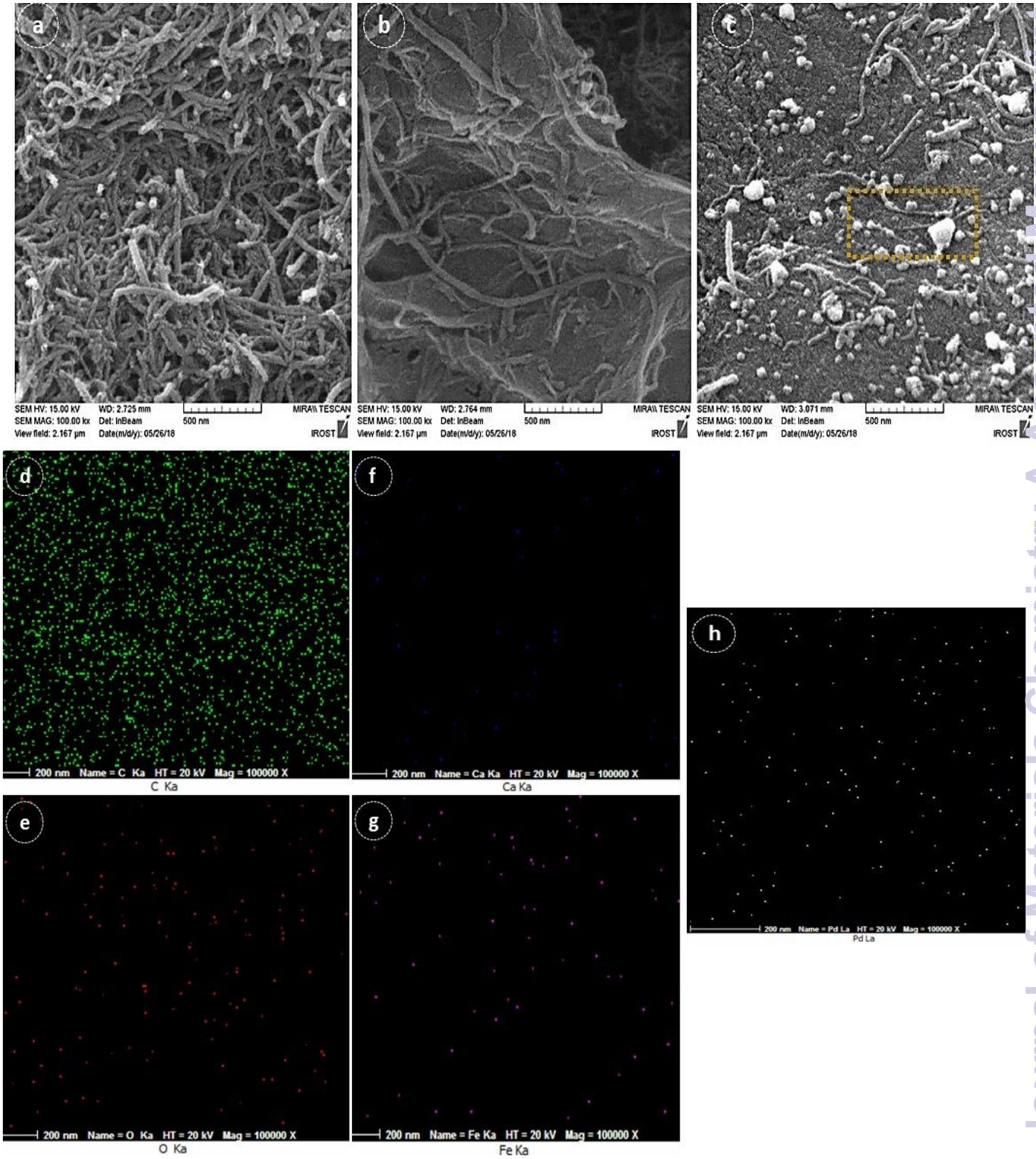

View Article Online
DOI: 10.1039/C9TA02882J

Fig. 2.

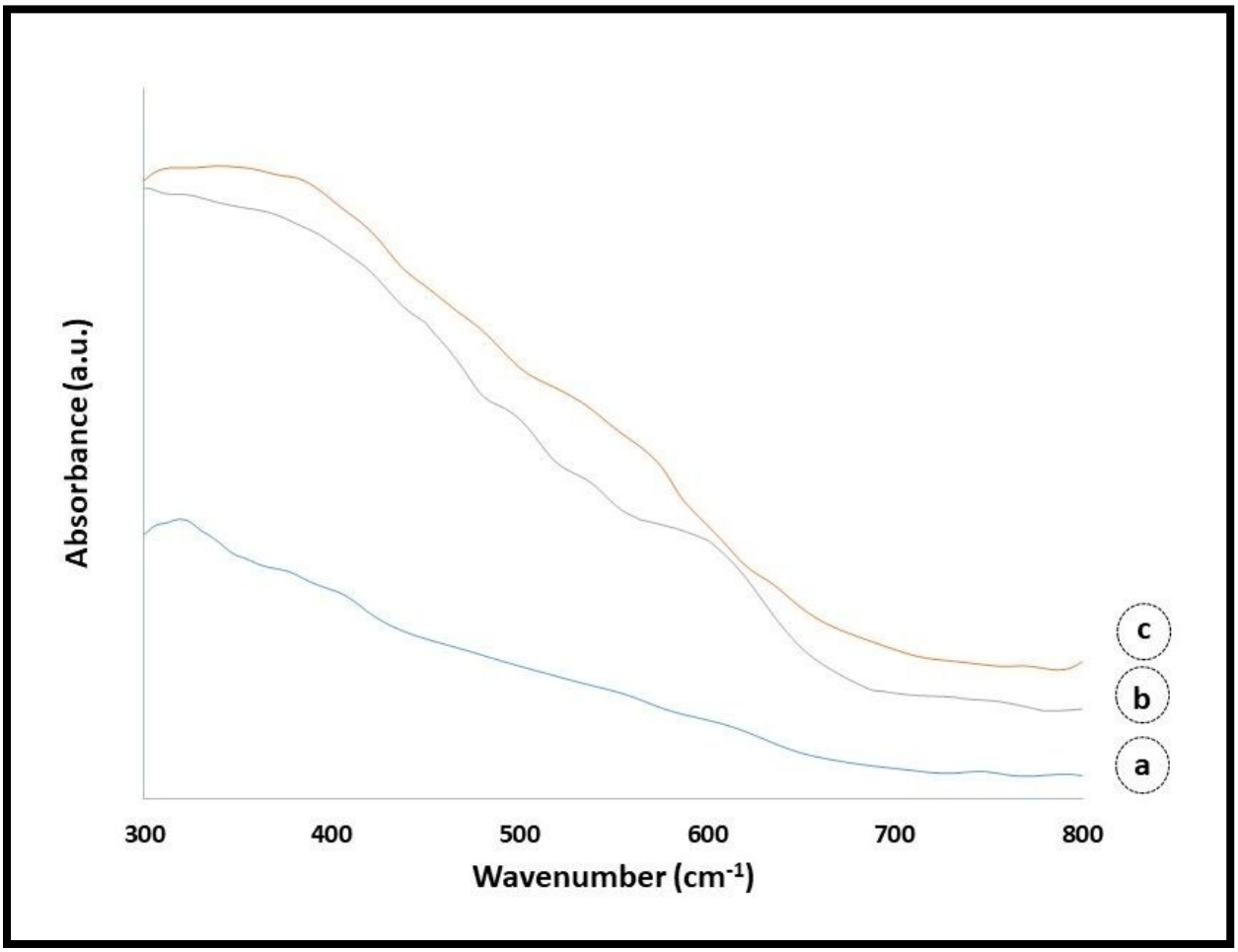

View Article Online
DOI: 10.1039/C9TA02882J

Fig. 3.

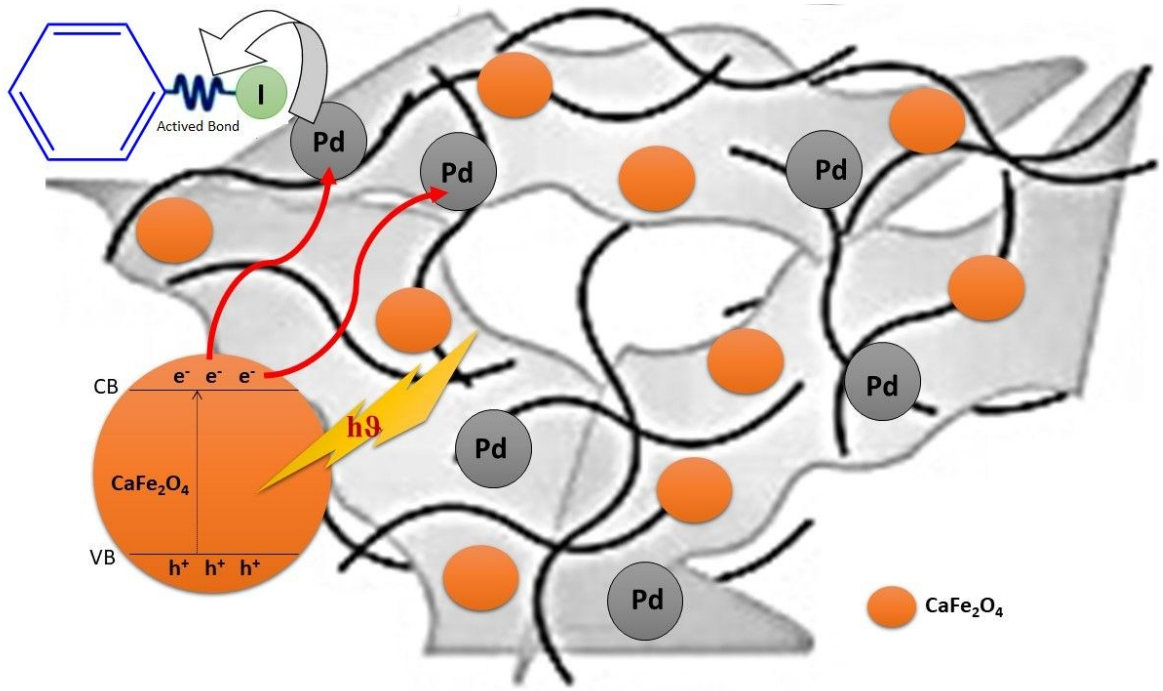

View Article Online
DOI: 10.1039/C9TA02882J

Fig. 4.[a]

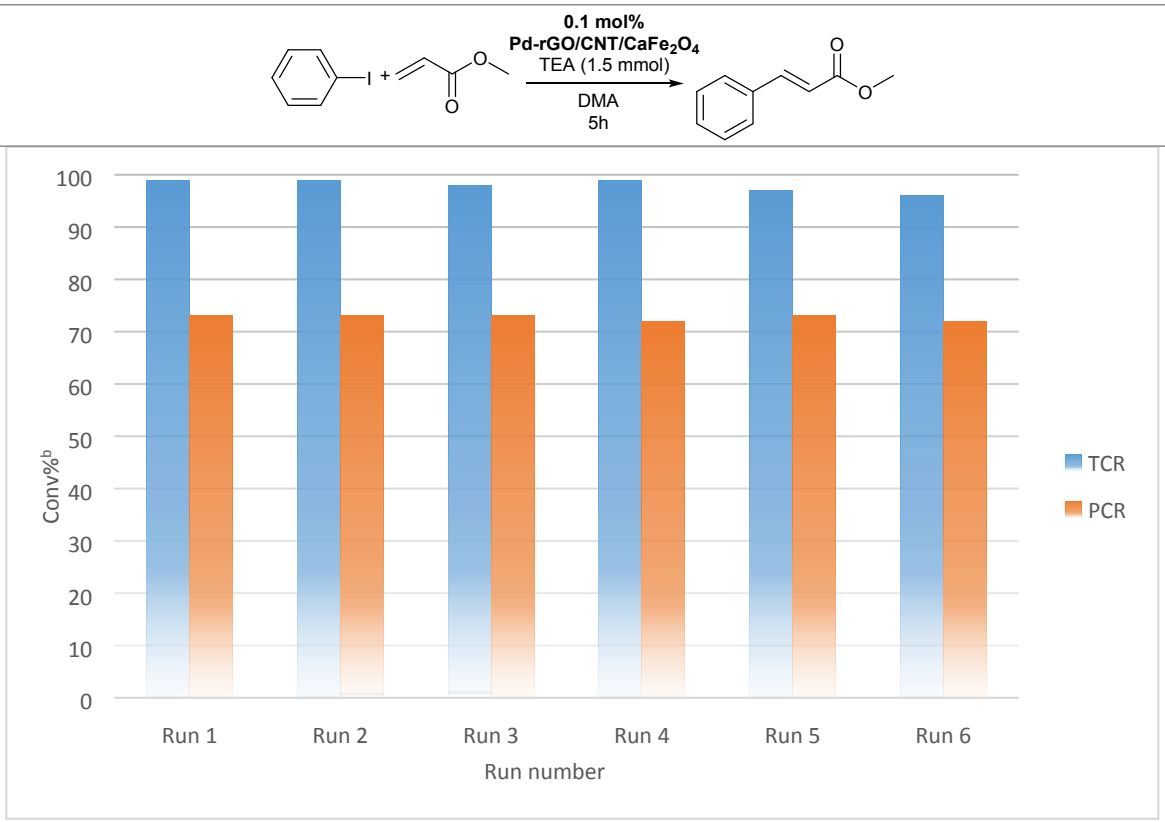

[a]; Reaction conditions: iodobenzene 1 mmol, methyl acrylate 1.2 mmol, TEA 1.5 mmol, 1 mL DMA and 5 h.
[b]; Measured by GC analyses.
TCR=Thermocatalytic Reaction; Conditions: 130 °C in dark environment.
PCR=Photocatalytic Reaction; Conditions: 25 °C controlled by water bath circulator under visible light illumination, a 250-W mercury lamp with the UV cut-off filter.

View Article Online
DOI: 10.1039/C9TA02882J

Table. 1.[a]

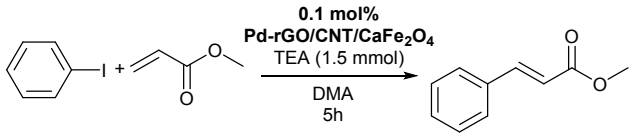

entry	mol % cat	Visible light	Temp.	Time	Conv[b]	Description
1	0.1	No	130 °C	5 h	>99%	Thermocatalytic Reaction[c]
2	0.1	Yes	25 °C	5 h	73%	Photocatalytic Reaction[d]
3	0.1	No	25 °C	5 h	0%	Dark control[e]

[a]; Reaction conditions: iodobenzene 1 mmol, methyl acrylate 1.2 mmol, TEA 1.5 mmol, 1 mL DMA and 5 h.
[b]; Measured by GC analyses.
[c]; 130 °C in a dark environment.
[d]; 25 °C controlled by water bath circulator under visible light illumination, a 250-W mercury lamp with the UV cut-off filter.
[c]; 25 °C controlled by water bath circulator in a dark environment.

View Article Online
DOI: 10.1039/C9TA02882J

Table. 2.[a]

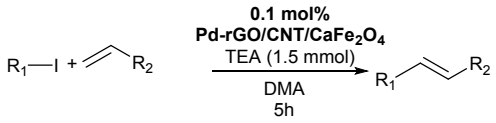

Entry	R_1	R_2	Product	Yield%[c] (TCR[d])	Yield%[c] (PCR[e])
1	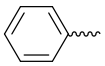		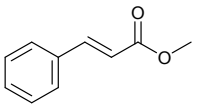	94	67
2	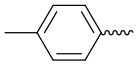		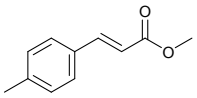	84	61
3	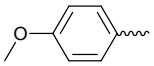		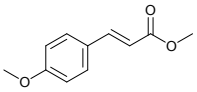	91	72
4	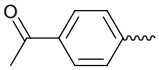		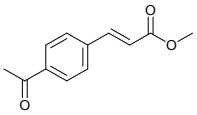	95	76
5	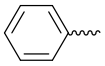	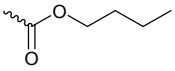	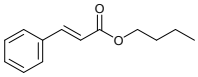	88	71
6	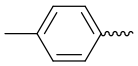	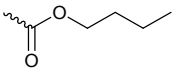	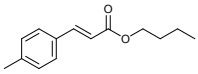	87	63
7	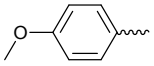	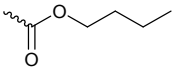	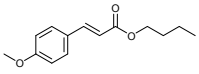	93	74
8	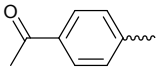	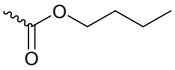	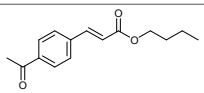	96	77
9	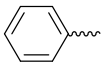		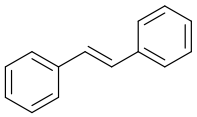	83	66
10	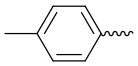		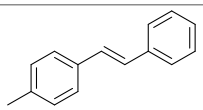	81	59
11	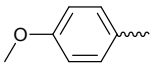		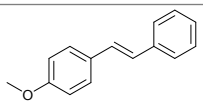	89	68

View Article Online
DOI: 10.1039/C9TA02882J

12	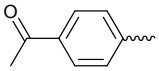		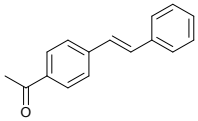	91	69
13	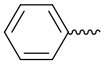	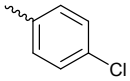	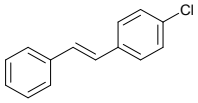	87	73
14	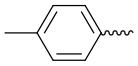	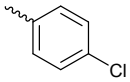	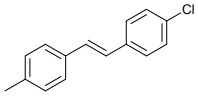	89	72
15	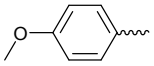	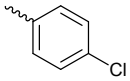	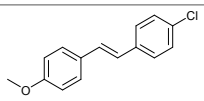	93	78
16	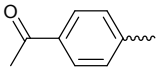	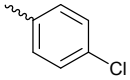	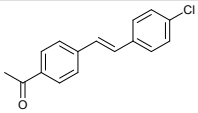	94	81

[a]; Reaction conditions: aryl iodide 1 mmol, olefin 1.2 mmol, TEA 1.5 mmol, 1 mL DMA and 5 h.
[c]; Isolated yield of the pure product after flash chromatography.
[d]; TCR=Thermocatalytic Reaction; conditions: 130 °C in dark environment.
[e]; PCR= Photocatalytic Reaction; conditions: 25 °C controlled by water bath circulator under visible light illumination, a 250-W mercury lamp with the UV cut-off filter.

View Article Online
DOI: 10.1039/C9TA02882J

Table. 3.[a]

entry	Catalytic system	Light source	Temperature (°C)	Time (h)	TOF (h^{-1})	Refrence
1	$PdCl_2/TiO_2$	UV-Vis	45	5	38.8	[27]
2	Pd/TiO_2	Vis (sun light)	r.t.	72	8.61	[8a]
3	Pd/CNCs	Vis	40	3	23.4	[28]
4	This work	Vis	r.t.	5	146	-

View Article Online
DOI: 10.1039/C9TA02882J

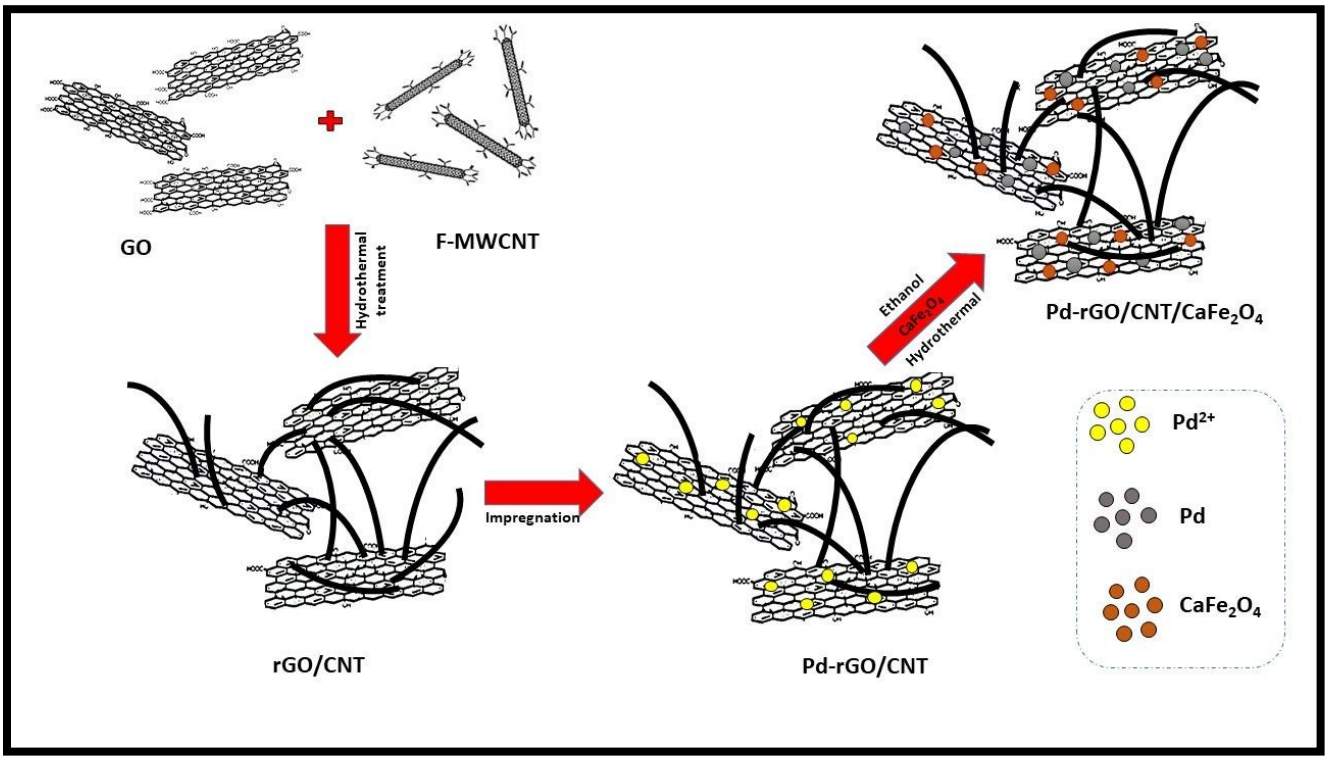

Scheme. 1. Schematic illustration of the preparation process of Pd-rGO/CNT/$CaFe_2O_4$ nanocomposite.

View Article Online
DOI: 10.1039/C9TA02882J

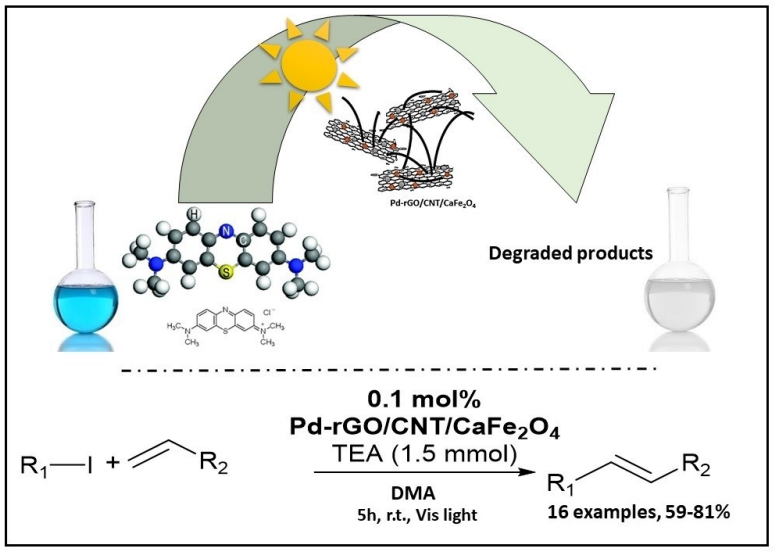

338x190mm (96 x 96 DPI)

View Article Online
DOI: 10.1039/C9TA02882J

Graphical Abstract

Facile synthesis of recyclable Pd-rGO/CNT/$CaFe_2O_4$ nanocomposite with high multifunctional photocatalytic activities under visible light irradiation

Mojtaba Bagherzadeh *, Reyhaneh Kaveh and Hamed Mahmoudi

A magnetically separable Pd-rGO/CNT/$CaFe_2O_4$ nanocomposite photocatalyst synthesized and its photocatalytic activity in the presence of visible-light were investigated. This photocatalyst not only presents remarkably increased photocatalytic activity toward MB degradation under visible irradiation but also presents significantly catalytic activity in Heck-Mizoroki coupling reactions under visible light to obtain the product in good to excellent yields. Moreover, the synthesized photocatalyst is so stable during the photocatalytic process.